Chapter 7

CHAPTER 7

MELEZITOSE - BASED SOLID – STATE BIOPOLYMER ELECTROLYTE AND ITS APPLICATION TO ELECTROCHEMICAL STORAGE DEVICES

To address future energy demands, it is indispensable to bring forth tunable energy storage devices from abundant materials in our environment. For decades, batteries are considered a valuable chemical energy conversion and storage device. Hence, searching for a healthier technology for the future using resourceful materials in nature will be a better feasible option. This leads to the development of biodegradable and sustainable energy storage devices. The biopolymers are abundant in nature, renewable, biodegradable, and biocompatible, and also offer shape and size profiles. Synthetic polymers have been replaced with biopolymers like pectin [1], cellulose acetate [2,3], chitosan [3], starch [4], iota, and kappa–carrageenan [5,6] as an alternative polymer host for a diversity of applications.

In the present investigation, Melezitose a biomolecule has been found in the ethanol extract of Corn Silk as evidenced in the GCMS data (Table 4.1). Melezitose (Mz) has been explored as the biomaterial for the preparation of the biopolymer electrolyte. This biomaterial is known for its existence in honeydews [7–9] as a component in honey and the crystallization of honey is due to this trisaccharide. Melezitose – "a forgotten sugar" has been found to exhibit numerous applications as a metabolic marker, excipient, lyoprotectant, surfactant, therapeutics, edibility enhancer, and more, but its competence in energy storage is still unfamiliar [10]. Hence, as a topic of interest, the presence of melezitose in Corn Silk Extract ignited the spark to explore its electrochemical applications.

7.1 *Investigation of Melezitose as solid bio-electrolyte for Mg-Ion Battery*

The structure of melezitose Mz is [O-α-D- glucopyranosyl-(1→ 3)-β-D-fructofuranosyl-(2 → 1)-α-D-glucopyranoside] [11] as depicted in Figure 7.1. This trisaccharide is derived from turanose which is an isomer of sucrose. This biomaterial Mz like sucrose holds many hydroxyl groups in its structure which can act as coordinating sites for the doped metallic salt. To decrease the brittleness and to increase the film-forming capacity of melezitose, polyvinyl alcohol (PVA) is blended. PVA is a versatile biopolymer with excellent mechanical and thermal properties. The blending of PVA with Mz improves the flexibility and elasticity of the prepared biopolymer (1g

Mz + 0.8g PVA). To facilitate its application to electrochemical devices and to reinforce ionic conductivity, magnesium perchlorate is chosen and incorporated with the prepared biopolymer.

On the lookout for biodegradable and sustainable energy devices, magnesium was the cost-effective and safe alternative with high earth abundance and environmentally friendly nature. To address the limitations of lithium, which is highly reactive to handle during the battery assembling session and is toxic to the environment, magnesium-based batteries are preferred. Magnesium has comparable ionic radii, smooth and dendrite-free mg deposition has a high volumetric capacity of 3832mAh $cm^{-3,}$ and is more stable than lithium even in humid atmospheres, supporting it to be a potential substitute to its lithium counterparts [12, 13]. The incorporation of magnesium salt into the biopolymer plays a crucial part in upgrading the ionic conductivity of the biopolymer electrolyte.

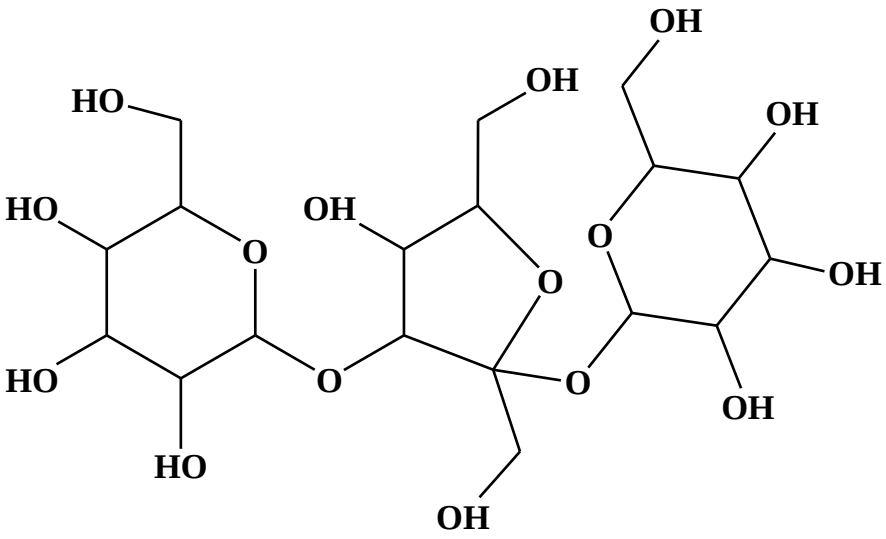

Figure 7.1: Structure of Melezitose

With this insight, a broad literature survey is performed. Hassan et al prepared a solid polymer electrolyte based on starch as the biopolymer and magnesium sulphate as the ionic dopant [14]. Kiruthika et al, reported a conducting biopolymer electrolyte using pectin and magnesium chloride as the dopant [15]. Also, Shanmugha Priya et al have studied the conductivity of the biopolymer electrolyte based on I-Carrageenan and magnesium nitrate [16]. Dannoun et al, synthesized magnesium ion-conducting blend polymer electrolytes using Chitosan: methylcellulose and magnesium acetate as the source of ions [17].

Zakaria R et al studied the conductivity of κ- Carrageenan – methylcellulose- NH_4I-based polymer electrolyte films prepared using a solution casting technique [18]. Perumal et al, have

employed a biomolecule tamarind seed polysaccharide for the preparation of the biopolymer electrolyte incorporating magnesium perchlorate [19]. The literature reports revealing that this present work is the first-ever report on Melezitose and the preparation of Melezitose: PVA blend (MZP) with magnesium perchlorate as the solid polymer electrolyte is completely novel.

7.1.1 Preparation of the blend solid biopolymer electrolyte MZP:

The biomaterial, melezitose lacks the film-forming tendency when it is made to film by a solution casting technique and hence PVA is used to prepare the biopolymer MZP. The biopolymer of melezitose is obtained by blending 1g Melezitose with 0.4g, 0.6g, 0.8g, and 0.9g PVA until sufficient blending since the conductivity of the biopolymer depends on the uniformity in mixing of the melezitose and PVA. The ionic conductivity of pure PVA is 2.5×10^{-10} Scm^{-1} [20,21] and that of the prepared biopolymer MZP is 9.85×10^{-6} Scm^{-1} which enunciates that the biomaterial melezitose has significantly contributed to the conductivity of the melezitose biopolymer. The biopolymer MZP of composition 1g Melezitose + 0.8g PVA, has been selected for further preparation of electrolyte, based on the conductivity values obtained from the corresponding Cole-Cole plot in Figures 7.7 and 7.8. The conductivity values for the prepared biopolymers are given in Table 7.1. Melezitose blend biopolymer (1g Melezitose + 0.8g PVA) and the biopolymer electrolytes are labeled as given in Table 1.10.

Table 7.1: Ionic conductivity (σ) values of the melezitose biopolymer at 303K

Composition	σ (S cm^{-1})	R_b (Ω)
1g Melezitose + 0.4g PVA	4.59×10^{-8}	339393
1g Melezitose + 0.6g PVA	6.71×10^{-7}	12857
1g Melezitose + 0.8g PVA	9.85×10^{-6}	854
1g Melezitose + 0.9g PVA	2.91×10^{-7}	46600

7.1.2 X-ray Diffraction (XRD) Analysis

XRD measurements has been performed for the biomaterial MZ, PVA, biopolymer MZP, and all the biopolymer electrolytes MMP1, MMP2, MMP3, MMP4, and MMP5. Figures 7.2 and 7.3 show the XRD patterns for MZ, PVA, MZP, MMP1, MMP2, MMP3, MMP4, and MMP5. The curve of Mz shows peaks at 2θ = 9.1°, 11.5°, 12.9°, 15.8°, 18°, 19.3°, 23.8°, 24.7°, 25.8°, 27.7°,

32.4°, 39.7°, and 48.9°. The XRD pattern for pure PVA in Figure 7.2 shows peaks at 19.4° and 40.4° which is similar to the results obtained by Manjuladevi et al [22]. The curve of MZP shows peak at 2θ = 9.1°, 11.4°, 12.6°, 15.8°, 18°, 19.4°, 23.8°, 24.3°, 25.6°, 27.5°, 32.0°, 39.47° and 48.8°. The intensity of the crystalline peaks in the curve MZP decreased due to the blending of PVA with Melezitose. The incorporation of Mg $(ClO_4)_2$ into the MZP biopolymer, further broadens the peak as seen in curve MMP1, where 2θ = 9.16°, 11.3°, 19.3°, 20.7°, and 27.8°. This decrease in intensity of the peak and increase in the broadness is due to the increase in the amorphous nature of the biopolymer due to the dissociation of salts in the biopolymer electrolytes. The XRD pattern for magnesium perchlorate as given by Ponmani et al [23] 2θ = 10.7°, 21.55°, 22.94°, 31.63°, 34.18°, 39.40°, 49.86°, 51.99, 55.41°. The XRD pattern of the magnesium perchlorate incorporated biopolymer electrolytes MMP2, MMP3, MMP4, and MMP5 in Figure 7.3 shows an increase in amorphous nature as seen in Table 7.2. The peaks for the magnesium perchlorate are almost absent in 1g Melezitose + 0.8g PVA + 0.8wt% Mg $(ClO_4)_2$. A peak observed at 22.4° in MMP1, MMP2, MMP3 for the Mg $(ClO_4)_2$ salt [24] has been absent in the highest conducting composition (1g Melezitose + 0.8g PVA + 0.8wt% Mg $(ClO_4)_2$) which again reappeared in MMP5. This also confirms the amorphous nature of MMP4.

Table 7.2: Percentage of crystallinity of MMP1, MMP2, MMP3, MMP4, MMP5

Composition	Percentage of Crystallinity
1g Melezitose + 0.8g PVA + 0.4wt% Mg $(ClO_4)_2$ (MMP1)	28.42
1g Melezitose + 0.8g PVA + 0.5wt% Mg $(ClO_4)_2$ (MMP2)	21.92
1g Melezitose + 0.8g PVA + 0.7wt% Mg $(ClO_4)_2$ (MMP3)	14.51
1g Melezitose + 0.8g PVA + 0.8wt% Mg $(ClO_4)_2$ (MMP4)	8.54
1g Melezitose + 0.8g PVA + 0.84wt% Mg $(ClO_4)_2$ (MMP5)	15.11

The degree of crystallinity decreases with the addition of 0.4wt% of Mg $(ClO_4)_2$ to 0.8wt% of Mg $(ClO_4)_2$ after which it increases with the increase in salt concentration. The addition of 0.4wt%, 0.5wt%, 0.7wt%, 0.8wt%, and 0.84wt% of Mg $(ClO_4)_2$ salt into the biopolymer MZP decreases the intensity of the peaks and also makes the hump broader and flatter, hence proving that the degree of amorphousity for the biopolymer increases [25].

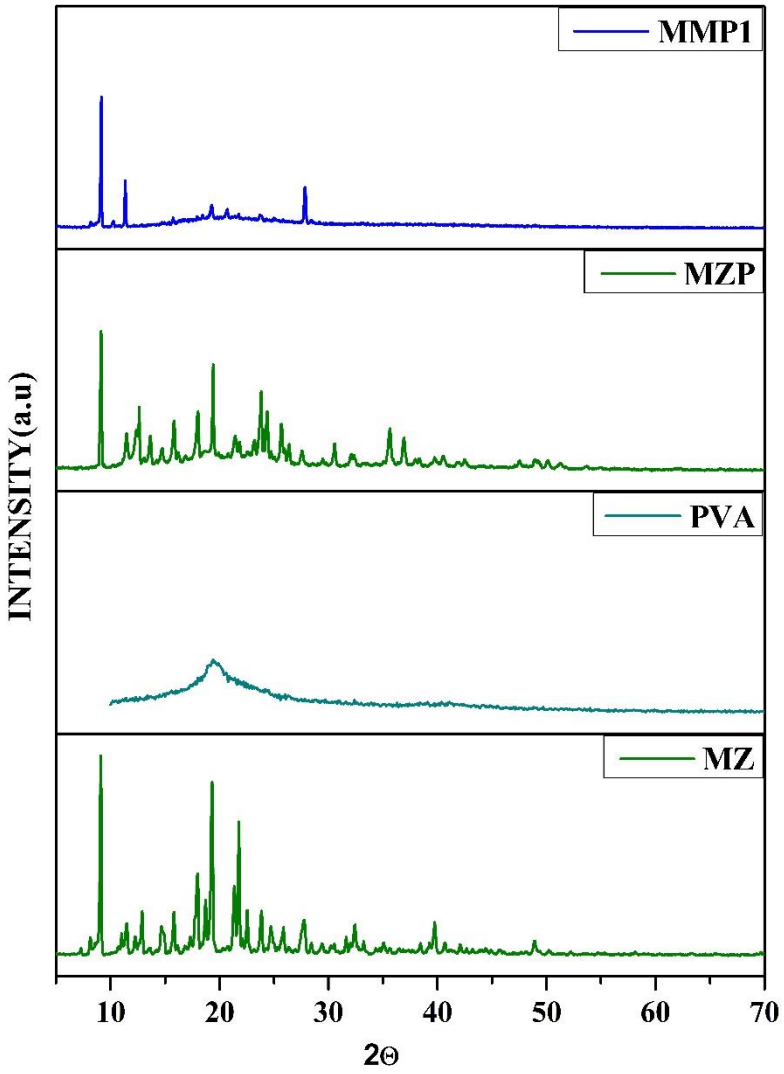

Figure 7.2: XRD pattern of MZ, PVA, MZP, and MMP1

Figure 7.3 for MMP4 demonstrates that the incorporation of Mg $(ClO_4)_2$ salt exhibits higher amorphousity compared to the other biopolymer electrolytes MMP1, MMP2, MMP3, MMP4, and MMP5. Thus, the high amorphous nature enables high ionic conductivity, and high ion carrier mobility, and reduces the energy barrier for the segmental motion of the biopolymer [26]. The decrease in the degree of crystallinity or increase in the amorphous nature of the electrolyte membrane is due to the complete dissociation of salts leading to the complexation of the biopolymer MZP with the salt. Since the energy barrier is low for ionic diffusivity in the amorphous state, the ions are free to move and hence ionic conductivity is high in a highly amorphous membrane [27].

This explains the high conductivity for the biopolymer electrolyte 1g Melezitose + 0.8g PVA + 0.8wt% Mg $(ClO_4)_2$. When the salt concentration added increases to 0.84wt%, there is an increase in intensity and a decrease in the broadness of the peak due to recrystallization of the Mg $(ClO_4)_2$ salt [28]. The degree of crystallinity has been calculated using the formula 3.2 from Chapter 3 and the values are given in Table 7.2.

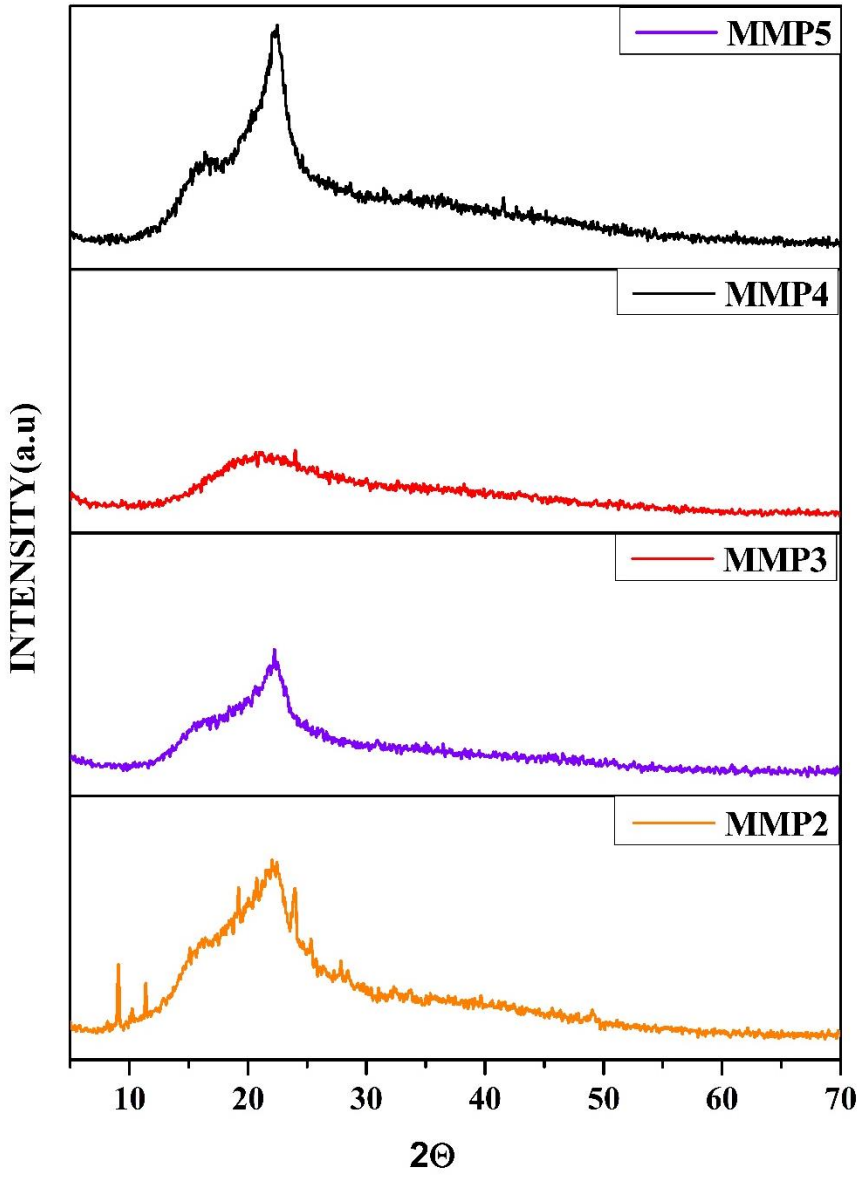

Figure 7.3: XRD pattern of MMP2, MMP3, MMP4, and MMP5

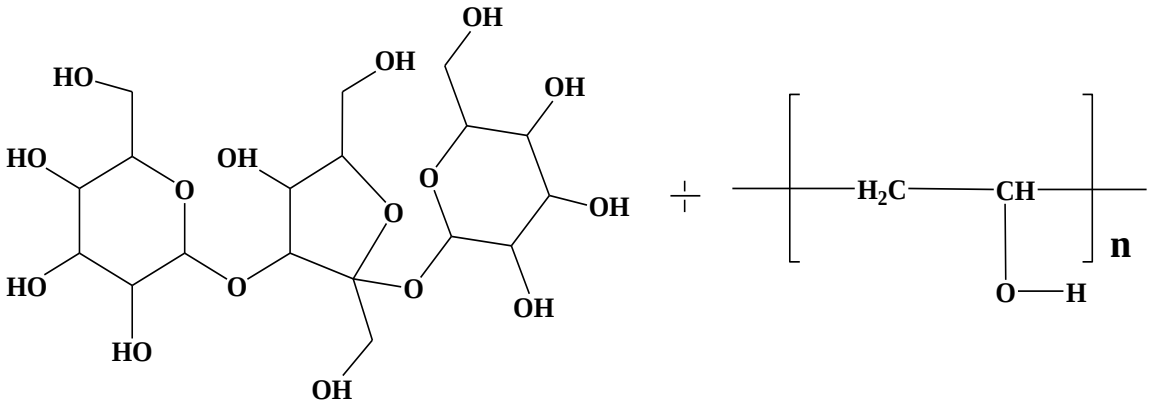

Melezitose **PVA**

Blending for 48hrs

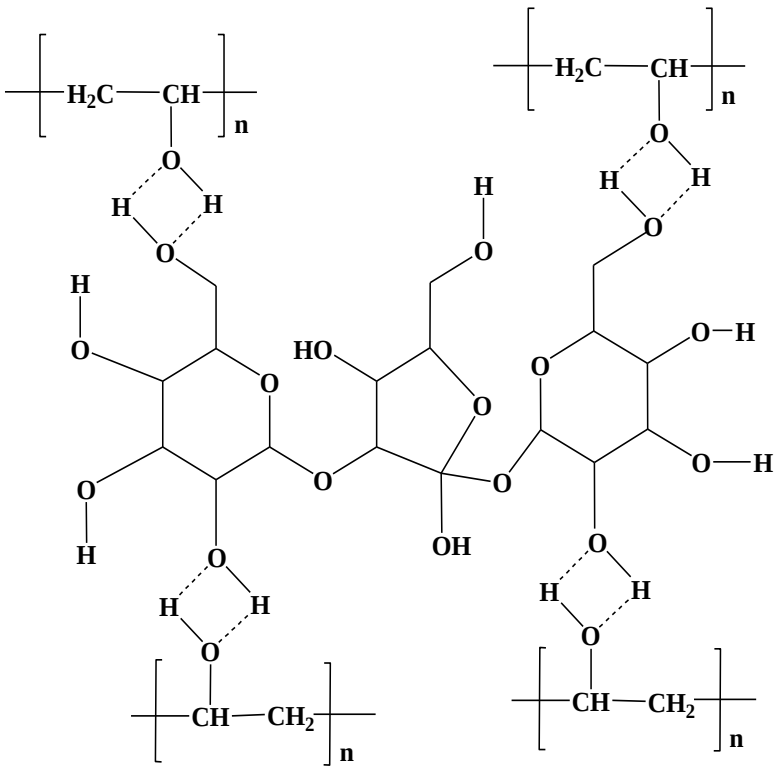

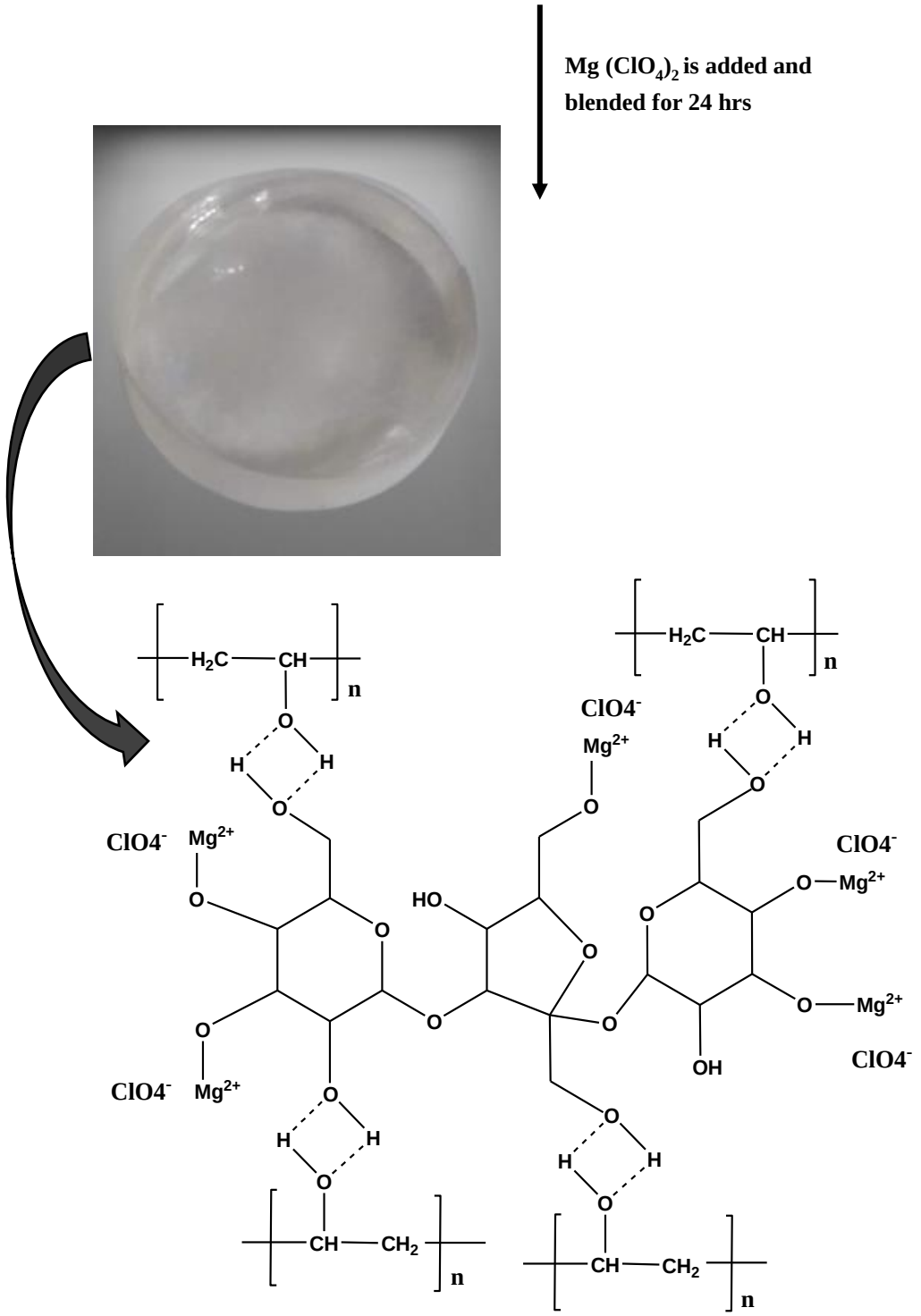

Figure 7.4: Predicted reaction mechanism between blend Melezitose, PVA and Magnesium perchlorate Salt

7.1.3 FTIR Spectra

The FTIR spectra of melezitose in Figure 7.5 A show the peak at 3779 cm^{-1} for the free – OH groups in its structure. A broad peak at 3388 cm^{-1} corresponds to the stretching vibrations of hydrogen-bonded OH groups. Another peak at 2354 cm^{-1} and 1592 cm^{-1} are attributed to – CH stretching and -OH bending vibrations. The peak at 1443 cm^{-1} and 1343 cm^{-1} are due to – CH_2 and – CH bending vibrations of the pyranose ring [29]. The peak at 1056 cm^{-1}, 990 cm^{-1}, and 912 cm^{-1} relates to the – C – OH linkage [30] and – C – O – C – linkages [31]. The peak around 671 cm^{-1} is due to the – OH out-of-plane bending vibrations. Figure 4b represents the IR spectra for the biopolymer MZP (1g Melezitose + 0.8g PVA). The peak at 3775 cm^{-1} corresponds to free OH groups and the intensity of the peak at 3388 cm^{-1} is reduced at 3332 cm^{-1} which evidenced the polymeric association of PVA with melezitose. Another peak at 2916 cm^{-1} that appeared in 4b is associated with the – CH_2 asymmetric stretching of PVA [32]. Similar peaks at 2354 cm^{-1} and 1592 cm^{-1} are obtained for – CH stretching and – OH bending vibrations. The broad peak corresponding to the – CH_2 and – CH bending vibrations of the pyranose ring is observed at 1443 cm^{-1} and 1343 cm^{-1}. The peaks at 988 cm^{-1}, 914 $cm^{-1,}$ and 1054 cm^{-1}corresponding to the C – O – C linkage and C – OH, and a peak at 683 cm^{-1} due to – OH out of plane bending is also observed.

Figure 7.5C - 7.5G represents the IR spectra for the biopolymer electrolyte doped with 0.4wt%, 0.5wt%, 0.7wt%, 0.8wt%, and 0.84wt% of Mg $(ClO_4)_2$. The peak at 3775 cm^{-1} and 3711 cm^{-1} in Figure 7.5B for the biopolymer disappeared in all the figures of the biopolymer electrolytes MMP1, MMP2, MMP3, MMP4, and MMP5 indicating the formation of the complex of Mg^{2+} ions with the hydroxide of the biopolymer. The peak around 2920 cm^{-1} associated with asymmetric – CH_2 stretching can be seen in Figure 7.5C - 7.5G at 2920 cm^{-1}, 2916 cm^{-1}, 2929 cm^{-1}, 2887 cm^{-1} and 2931 cm^{-1}. Also, the intensity of the peak seen at 2354 cm^{-1} in 4b is found to decrease in all the figures from 7.5C - 7.5G which is also a confirmation of the complex of the salt with the biopolymer. The peak for – OH bending vibration observed at 1592 cm^{-1} in Figure 7.5B can be seen in figures 7.5C - 7.5G with reduced intensity and lower wavenumber from 1643 cm^{-1} to 1637 cm^{-1}. The – CH_2 bending vibrations of the pyranose ring and – CH bending vibrations found at 1443 cm^{-1} and 1343 cm^{-1} were found as the less intense peak in figures 7.5C - 7.5G at 1308 cm^{-1} and 1273 cm^{-1} respectively. The corresponding vibrational frequencies are listed in Table 7.3.

The peaks at 1054 cm^{-1} in Figure 7.5B for – C – OH linkage [33] are found to be more intense peaks in figure 7.5C - 7.5G at 1052 cm^{-1}, 1040 cm^{-1}, 1058 cm^{-1}, 1027 $cm^{-1,}$ and 1062 $cm^{-1,}$ and the C – O – C peak in Figure 7.5B at 988 cm^{-1} and 914 cm^{-1} is seen as less intense peaks

in all the biopolymer electrolyte plots and disappeared at MMP5 composition in Figure 7.5F. A peak appeared at 617 cm^{-1} in Figure 7.5C in all Mg $(ClO_4)_2$ incorporated samples, evidenced by the presence of a C – Cl stretching peak [34]. This peak ascribed to C – Cl is also seen in figures 7.5D - 7.5G at 615 cm^{-1}, 615 cm^{-1}, 595 $cm^{-1,}$ and 615 cm^{-1} respectively. These results predict the complex formation of the salt magnesium perchlorate with the host biopolymer MZP and the predicted mechanism for the integration of the melezitose, PVA and magnesium perchlorate salt is illustrated in Figure 7.4.

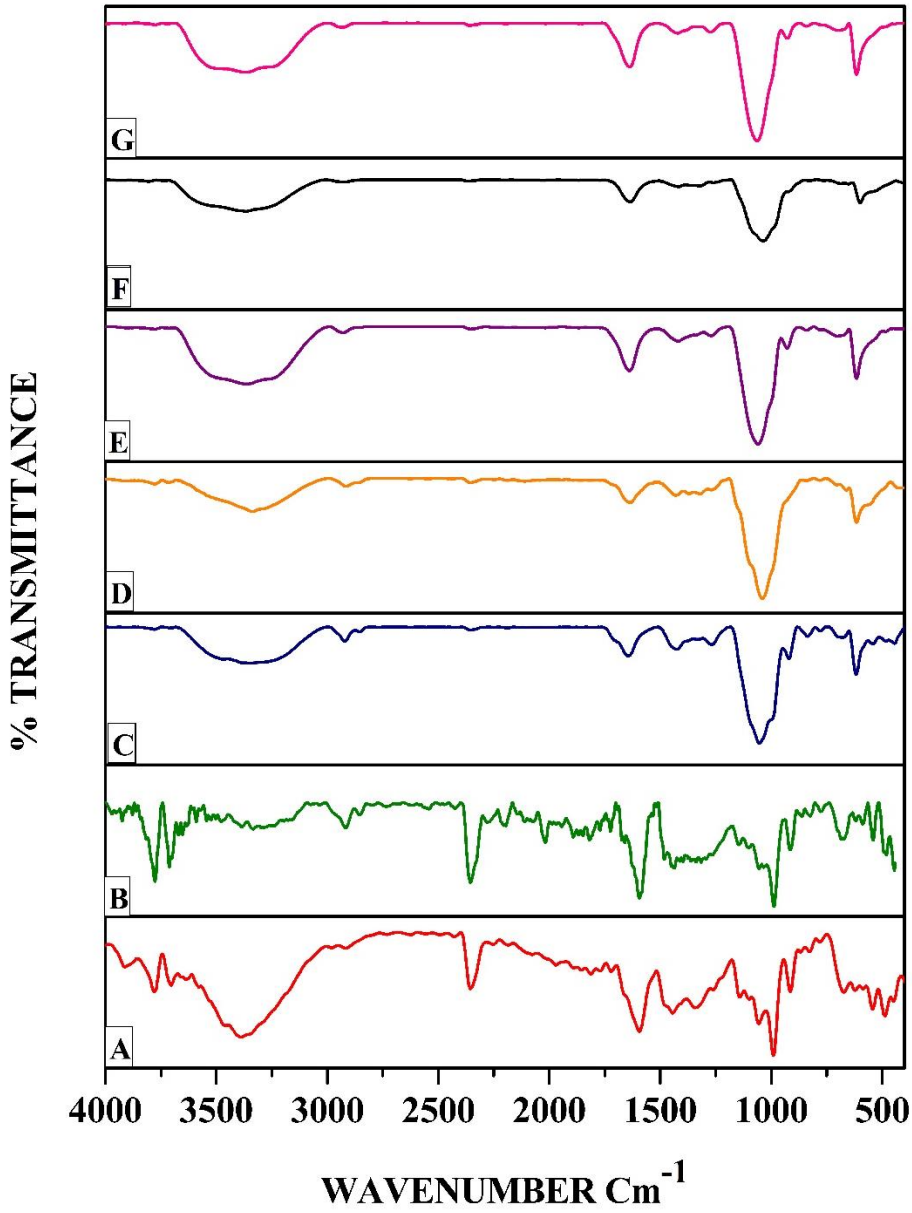

Figure 7.5: FT – IR spectra of Mz (A), MZP (B), MMP1 (C), MMP2 (D), MMP3 (E), MMP4 (F), and MMP5 (G)

Assignments	MZ	MZP	MMP1	MMP2	MMP3	MMP4	MMP5
Free OH group	3779cm^{-1}	3775 cm^{-1}	-	-	-	-	-
H bonded –OH	3388 cm^{-1}	3332 cm^{-1}	3378 cm^{-1}	3336 cm^{-1}	3367 cm^{-1}	3326 cm^{-1}	3367 cm^{-1}
–CH_2 asymmetric stretching	-	2916cm^{-1}	2920 cm^{-1}	2916 cm^{-1}	2929 cm^{-1}	2887 cm^{-1}	2931 cm^{-1}
–CH stretching	2354cm^{-1}	2354cm^{-1}	2354 cm^{-1}	2354 cm^{-1}	2354 cm^{-1}	2337 cm^{-1}	2358 cm^{-1}
–OH bending	1592cm^{-1}	1592 cm^{-1}	1643 cm^{-1}	1637 cm^{-1}	1637 cm^{-1}	1619 cm^{-1}	1637 cm^{-1}
–CH_2 and –CH bending vibration of pyranose ring	1443 cm^{-1} & 1343cm^{-1}	1443 cm^{-1} & 1343 cm^{-1}	1423 cm^{-1} & 1266 cm^{-1}	1431 cm^{-1} & 1320 cm^{-1}	1419 cm^{-1} & 1270 cm^{-1}	1402 cm^{-1} & 1308 cm^{-1}	1421 cm^{-1} & 1273 cm^{-1}
C–O–H & C–O–C	1056 cm^{-1} & 990 cm^{-1}, 912 cm^{-1}	1054 cm^{-1} & 988 cm^{-1}, 914 cm^{-1}	1052 cm^{-1} & 918 cm^{-1}	1040 cm^{-1}	1058 cm^{-1}	1027 cm^{-1}	1062 cm^{-1} & 926 cm^{-1}
–OH out of plane bending	671 cm^{-1}	683 cm^{-1}	-	-	-	-	-
C–Cl	-	-	617 cm^{-1}	615 cm^{-1}	615 cm^{-1}	595 cm^{-1}	615 cm^{-1}

Table 7.3: Peak position and vibrational Assignments of Pure MZP and Mg $(ClO_4)_2$ incorporated biopolymers

7.1.4 Differential Scanning Calorimetry (DSC)

The change in the glass transition temperature of the biopolymer electrolyte system is analyzed using differential scanning calorimetry. Figure 7.6 shows the thermograms of the pure biomaterial MZ, its PVA blended biopolymer MZP, and $Mg(ClO_4)_2$ incorporated biopolymer electrolytes MMP1, MMP2, MMP3, MMP4, and MMP5. The glass transition temperatures of Melezitose, its blend MZP, and the biopolymer electrolytes are listed in Table 7.4.

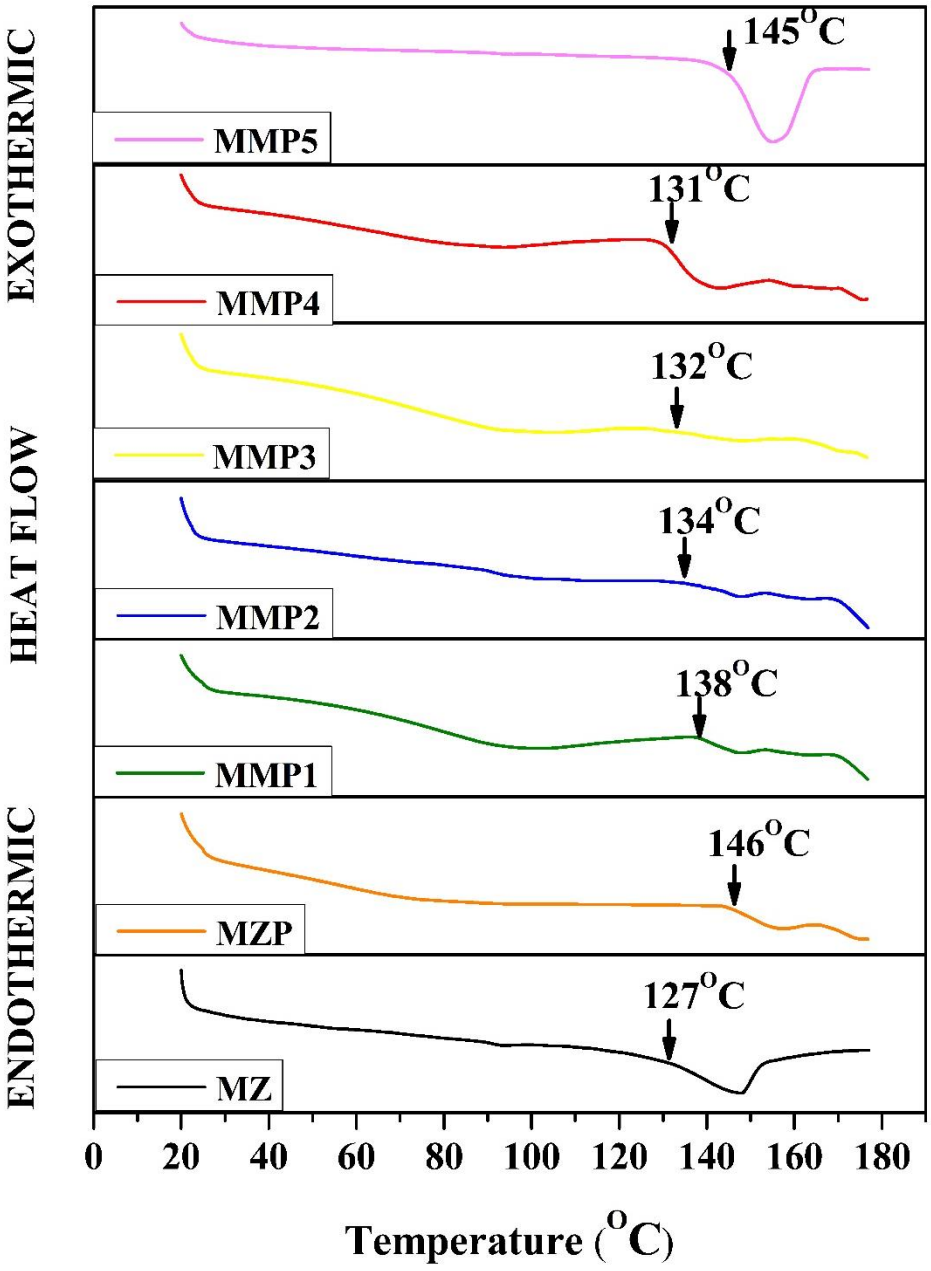

Figure 7.6: DSC thermogram of Mz, MZP, MMP1, MMP2, MMP3 , MMP4 , and MMP5

The pure melezitose MZ has a glass transition temperature value of 127°C whereas the PVA blended biopolymer MZP, has a T_g value of 146°C. The trend in the T_g value shows a decrease for MMP1, MMP2, MMP3, and MMP4 with the addition of 0.4wt%, 0.5wt%, 0.7wt%, and 0.8wt% of Mg $(ClO_4)_2$. The decrease in T_g is a suggestion about the plasticizing nature of the magnesium perchlorate salt [22]. When the salt is added to the biopolymer MZP, it breaks the transient coordinate bonds among the melezitose, and PVA blend, through its complexation with the polymer chains. Thus, adding an increasing concentration of magnesium perchlorate weakens the dipole-dipole interactions among the biopolymer backbone and improves the mobility of the biopolymer backbone. Enhanced ionic conductivity for the biopolymer electrolyte at low T_g with MMP4 composition is due to the increased segmental motion in the biopolymer electrolyte [35].

COMPOSITION	T_g
MZ	127.16°C
MZP	146.55°C
MMP1	138.76°C
MMP2	134.59°C
MMP3	132.31°C
MMP4	**131.67°C**
MMP5	145.22°C

Table 7.4: Glass transition temperature of MZ, MZP, and Mg $(ClO_4)_2$ incorporated biopolymers

Later, further addition of the magnesium perchlorate to the biopolymer MMP5 leads to an increase in glass transition temperature to 145°C. This is due to the formation of undissociated salt in the biopolymer electrolyte [36, 34]. These ionic clusters developed in the electrolyte limits the movement of ions due to the lowering of rubbery nature and thus increase the T_g of MMP5 [37]. Comparative results have been stated by Mahalakshmi et al [38] for 60:40 % composition of CA: $Mg(ClO_4)_2$ and Manjuladevi et al [22] for the composition of 92.5PVA:7.5PAN:0.25% $Mg(ClO_4)_2$.

7.1.5 AC Impedance Spectroscopy

Figure 7.7 shows the Cole-Cole plot for the pure biopolymer MZP. Figures 7.9 and 7.10 show the Cole-Cole plot for the biopolymer electrolytes MMP1, MMP2, MMP3, MMP4, and MMP5 respectively. From the plots, we can observe two well-defined regions, that is a high-

frequency semicircle region and a low-frequency inclined spike region. In Figure 7.7, it is clear that the semicircle has disappeared and only a spike region is noticed. This interprets that the blend biopolymer has only a resistive component and it originated due to the arbitrary arrangement of the polar groups in the melezitose and PVA backbone. The ionic conductivity (σ) is calculated by using equation 3.5 as discussed in Chapter 3.

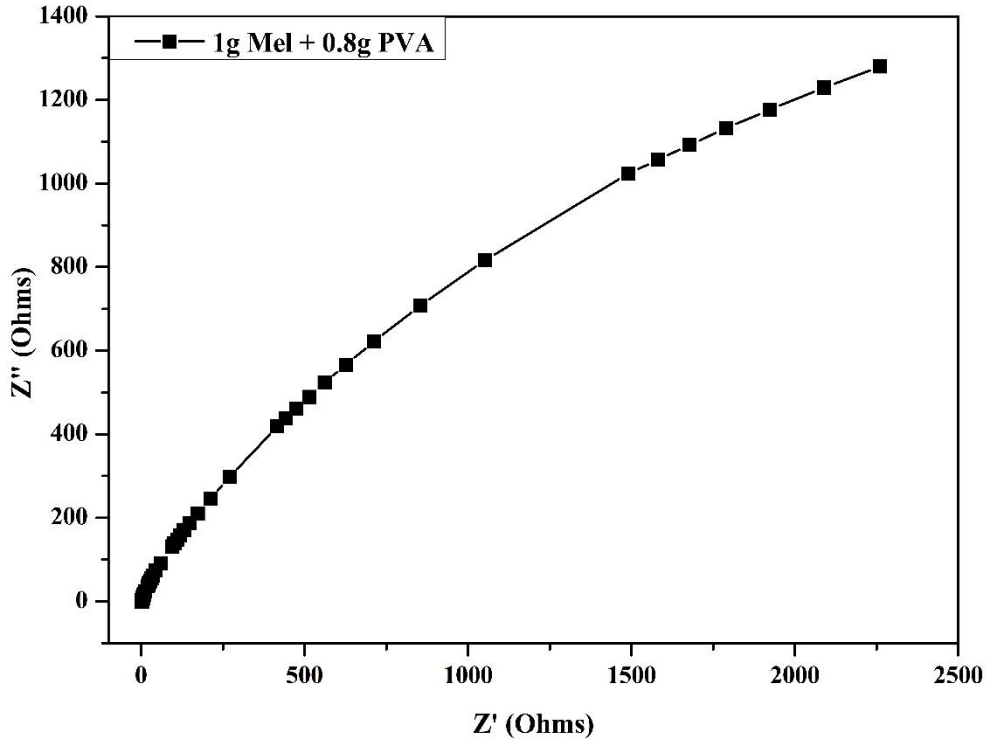

Figure 7.7: Cole-Cole plot for the biopolymer membrane MZP (1g Mel + 0.8g PVA)

The ionic conductivity of the blend pure biopolymer MZP (1g Melezitose + 0.8g PVA) is 9.8×10^{-6} Scm^{-1} and is selected for the preparation of the biopolymer electrolyte with $Mg(ClO_4)_2$ as the dopant. Figure 7.9 and 7.10 shows the Cole-Cole plot for the biopolymer electrolyte with different concentrations of $Mg(ClO_4)_2$. Bulk resistance for each electrolyte is computed by using EQ Software of B.A. Boukamp in Table 7.5 [39, 40]. Figure 7.10 shows the plot for the highest conducting electrolyte has a spike with a very small and depressed semicircle. This indicates the effect between two blocking electrodes representing the formation of the double-layer capacitance of the biopolymer electrolyte film interface [33]. The value of bulk resistance decreased with the addition of $Mg(ClO_4)_2$ until the composition MMP4 and after which R_b value started to increase. The semicircle in the high-frequency region fades away gradually with 0.8wt% of magnesium

perchlorate, suggesting that the resistive component of the biopolymer electrolyte can be considered.

The enhanced conductivity from 8.49×10^{-5} Scm^{-1} to 1.44×10^{-3} Scm^{-1} on the addition of 0.4wt%, 0.5wt%, 0.7wt%, 0.8wt%, and 0.84wt% of magnesium perchlorate is due to improvement of ionic mobility and the number of charge carrier ions [33].

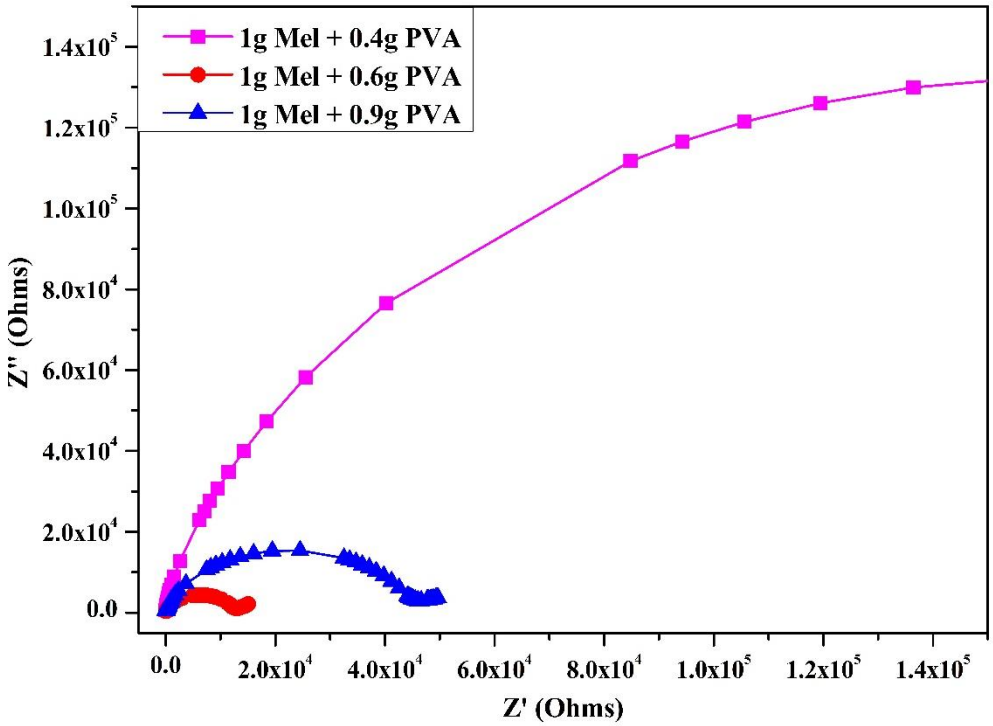

Figure 7.8: Cole-Cole plots for the biopolymer membranes (1g Mel + 0.4g PVA), (1g Mel + 0.6g PVA), and (1g Mel + 0.9g PVA)

Table 7.5: Ionic conductivity (σ) values of the melezitose biopolymer electrolvtes at 303K

Composition	**σ (S cm^{-1})**	**R_b (Ω)**
1g Melezitose + 0.8g PVA	9.85×10^{-6}	854
1g Melezitose + 0.8g PVA + 0.4wt% Mg $(ClO_4)_2$	8.49×10^{-5}	226
1g Melezitose + 0.8g PVA + 0.5wt% Mg $(ClO_4)_2$	1.02×10^{-4}	248
1g Melezitose + 0.8g PVA + 0.7wt% Mg $(ClO_4)_2$	7.25×10^{-4}	18
1g Melezitose + 0.8g PVA + 0.8wt% Mg $(ClO_4)_2$	1.44×10^{-3}	6
1g Melezitose + 0.8g PVA + 0.84wt% Mg $(ClO_4)_2$	7.24×10^{-4}	44

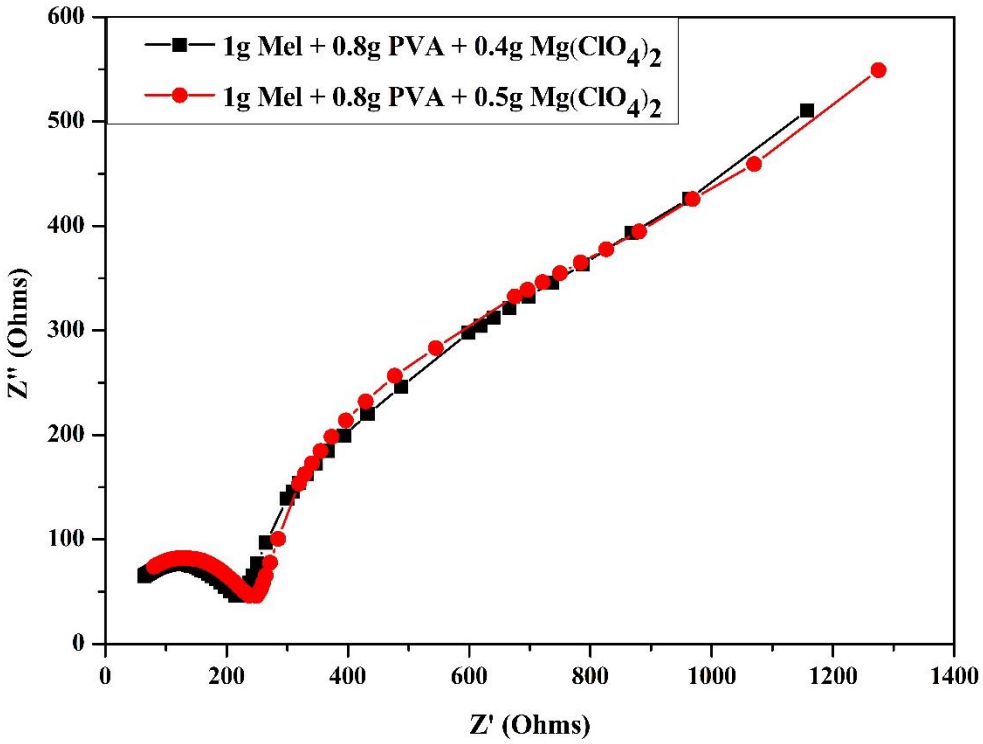

Figure 7.9: Nyquist plot for MMP1, MMP2 at room temperature

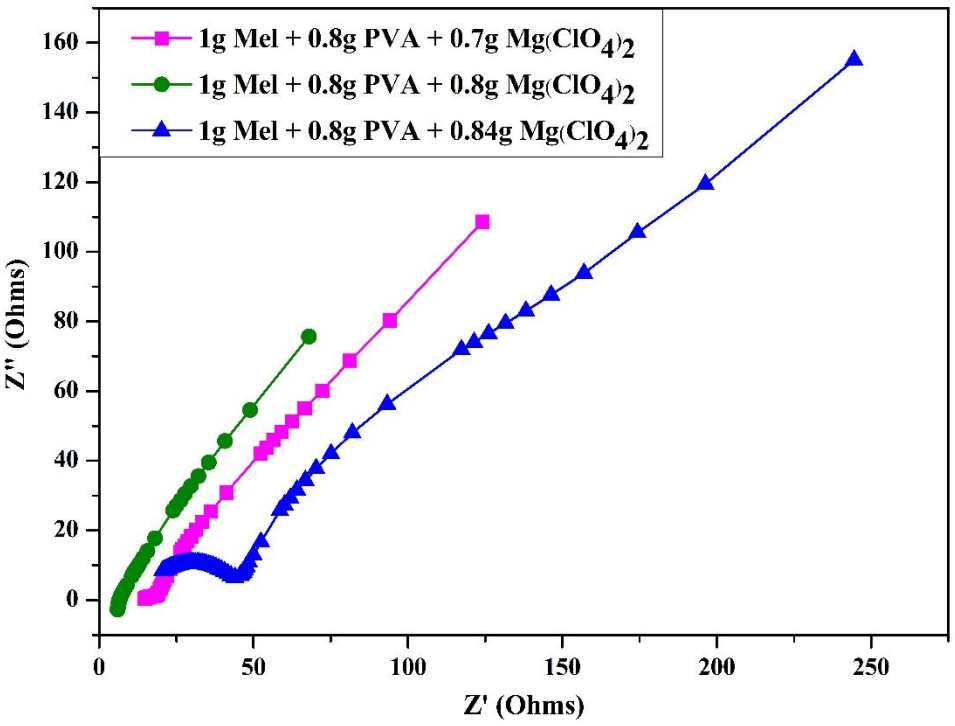

Figure 7.10: Nyquist plot for MMP3, MMP4, and MMP5 at room temperature

References

[1] S. Kiruthika, M. Malathi, S. Selvasekarapandian, K. Tamilarasan, T. Maheshwari, Polymer Bulletin 77 (2020) 6299–6317.

[2] S. Monisha, T. Mathavan, & S. Selvasekarapandian, & A. Milton, F. Benial, & M. Prema Latha, Ionics 23 (2017) 2697–2706.

[3] P. Adlin Helen, P. Perumal, P. Sivaraj, M. Infanta Diana, P. Christopher Selvin, Mater Today Proc (2020).

[4] M.F. Shukur, F. Sonsudin, R. Yahya, Z. Ahmad, R. Ithnin, M.F.Z. Kadir, in: Adv Mat Res, 2013, pp. 120–124.

[5] S. Shanmuga Priya, M. Karthika, S. Selvasekarapandian, R. Manjuladevi, S. Monisha, Ionics (Kiel) 24 (2018) 3861–3875.

[6] P. Sangeetha, T.M. Selvakumari, S. Selvasekarapandian, S.R. Srikumar, R. Manjuladevi, M. Mahalakshmi, Ionics (Kiel) 26 (2020) 233–244.

[7] P.K. Nguyen, J.E. Owens, L.E. Lowe, E.H. Mooney, 7 (2020).

[8] V.C. Seeburger, P. D'Alvise, B. Shaaban, K. Schweikert, G. Lohaus, A. Schroeder, M. Hasselmann, PLoS One 15 (2020).

[9] M. Lenaerts, L. Abid, C. Paulussen, T. Goelen, F. Wäckers, H. Jacquemyn, B. Lievens, J Chem Ecol 42 (2016) 1028–1036.

[10] P. Behera, S. Balaji, Carbohydr Res 500 (2021) 108248.

[11] B.J. S D Bacon, B. Dickinson, Carbohydrate metabolism of skin 289 The Origin of Melezitose: A Biochemical Relationship between the Lime Tree (Tilia Spp.) and an Aphis (Eucallipterus Tiliae L.), The Year Book Publishers Inc, 1941.

[12] Y. Shao, N.N. Rajput, J. Hu, M. Hu, T. Liu, Z. Wei, M. Gu, X. Deng, S. Xu, K.S. Han, J. Wang, Z. Nie, G. Li, K.R. Zavadil, J. Xiao, C. Wang, W.A. Henderson, J.G. Zhang, Y. Wang, K.T. Mueller, K. Persson, J. Liu, Nano Energy 12 (2015) 750–759.

[13] M.S.A. Rani, N.S. Isa, M.H. Sainorudin, N.A. Abdullah, M. Mohammad, N. Asim, H. Razali, M.A. Ibrahim, Int J Electrochem Sci 16 (2021) 1–10.

[14] M.F. Hassan, N.S.N. Azimi, K.H. Kamarudin, C.K. Sheng, Solid Polymer Electrolytes Based on Starch-Magnesium Sulphate: Study on Morphology and Electrical Conductivity, 2018.

[15] S. Kiruthika, M. Malathi, S. Selvasekarapandian, K. Tamilarasan, T. Maheshwari, Polymer Bulletin 77 (2020) 6299–6317.

[16] S. Shanmuga Priya, M. Karthika, S. Selvasekarapandian, R. Manjuladevi, Solid State Ion 327 (2018) 136–149.

[17] E.M.A. Dannoun, S.B. Aziz, M.A. Brza, M.M. Nofal, A.S.F.M. Asnawi, Y.M. Yusof, S. Al-Zangana, M.H. Hamsan, M.F.Z. Kadir, H.J. Woo, Polymers (Basel) 12 (2020) 1–19.

[18] R. Zakaria, A.M.M. Ali, Scientific Research Journal 17 (2020) 119.

[19] P. Perumal, K.P. Abhilash, P.Sivaraj, P.C. Selvin, Mater Res Bull 118 (2019).

[20] G. Hirankumar, S. Selvasekarapandian, M. Bhuvaneswari, R. Baskaran, M. Vijayakumar, AC Impedance Studies on Proton Conducting Polymer Electrolyte Complexes (PVA+CH3COONH 4), 2004.

[21] V. Parameswaran, N. Nallamuthu, P. Devendran, E.R. Nagarajan, A. Manikandan, Physica B Condens Matter 515 (2017) 89–98.

[22] R. Manjuladevi, M. Thamilselvan, S. Selvasekarapandian, R. Mangalam, M. Premalatha, S. Monisha, Solid State Ion 308 (2017) 90–100.

[23] S. Ponmani, B. Susithra, M.R. Prabhu, International Journal of Advance Engineering and Research Development International Conference on Momentous Role of Nanomaterials in Renewable Energy Devices 5 (2018).

[24] Reddy, M. Jaipal, and Peter P. Chu.Solid State Ionics 149 (2002) 115-123.

[25] R. Manjuladevi, M. Thamilselvan, S. Selvasekarapandian, R. Mangalam, M. Premalatha, S. Monisha, Solid State Ion 308 (2017) 90–100.

[26] P. Perumal, S. Selvasekarapandian, K.P. Abhilash, P. Sivaraj, R. Hemalatha, P.C. Selvin, Vacuum 159 (2019) 277–281.

[27] M.Y.A. Rahman, A. Ahmad, T.K. Lee, Y. Farina, H.M. Dahlan, J Appl Polym Sci 124 (2012) 2227–2233.

[28] S. Monisha, T. Mathavan, S. Selvasekarapandian, A.M.F. Benial, M.P. latha, Ionics (Kiel) 23 (2017) 2697–2706.

[29] El-Sakhawy, M., Kamel, S., Salama, A., & Tohamy, H. A. S.Cellul. Chem. Technol, 52 (2018) 193-200.

[30] M. Kanou, K. Nakanishi, A. Hashimoto, T. Kameoka, Influences of Monosaccharides and Its Glycosidic Linkage on Infrared Spectral Characteristics of Disaccharides in Aqueous Solutions, 2005.

[31] N.A. Nikonenko, D.K. Buslov, N.I. Sushko, R.G. Zhbankov, B.I. Stepanov. Biopolymers. 57 (2000) 257-62.

[32] R. Manjuladevi, M. Thamilselvan, S. Selvasekarapandian, P. Christopher Selvin, R. Mangalam, S. Monisha, Ionics (Kiel) 24 (2018) 1083–1095.

[33] I. Min, Ionic Conductivity and Conduction Mechanism Studies of CMC/ Chitosan Biopolymer Blend Electrolytes, 2014.

[34] M. Mahalakshmi, S. Selvanayagam, S. Selvasekarapandian, V. Moniha, R. Manjuladevi, P. Sangeetha, Journal of Science: Advanced Materials and Devices 4 (2019) 276–284.

[35] S. Selvasekarapandian, Preparation and characterization of biopolymer based on dextran and poly (vinyl alcohol), 2019.

[36] C.W. Liew, S. Ramesh, Carbohydr Polym 124 (2015) 222–228.

[37] P. Perumal, K.P. Abhilash, P.Sivaraj, P.C. Selvin, Mater Res Bull 118 (2019).

[38] M. Mahalakshmi, S. Selvanayagam, S. Selvasekarapandian, V. Moniha, R. Manjuladevi, P. Sangeetha, Journal of Science: Advanced Materials and Devices 4 (2019) 276–284.

[39] B.A. Boukamp, A package for impedance/admittance data analysis. Solid State Ionics (1986) 136-140.

[40] B.A. Boukamp, A nonlinear least squares fit procedure for analysis of immittance data of electrochemical systems, Solid State Ionics 20 (1986) 31-44.